X International Conference on Computational Methods in Marine Engineering
MARINE 2023
J. Garcia-Espinosa, L. González, J.E. Gutiérrez & B. Serván-Camas (Editors)

Numerical Study of Cavitation on a Ship Propeller in Regular Waves of Different Headings

MARINE 2023

Keun Woo Shin[1*], Henrik Mikkelsen[2], Yanlin Shao[3], Jens Honore Walther[3] and Jens Ring Nielsen[1]

[1] Propeller & Aftship R&D Department, MAN Energy Solutions, Frederikshavn, Denmark. http://www.man-es.com

[2] Aerotak, Kgs. Lyngby, Denmark. http://www.aerotak.dk

[3] Department of Mechanical Engineering, Technical University of Denmark (DTU), Kgs. Lyngby, Denmark. http://www.mek.dtu.dk

[*] Corresponding author: Keun Woo Shin, keun.shin@man-es.com

ABSTRACT

As ships operate under sea wave conditions most of time, it is desirable to consider the wave effect on propeller performance and cavitation safety in the propeller design process. In this work, unsteady cavitation simulations are carried out on a five-bladed propeller of KRISO container ship in calm water and regular waves of five different headings. Bare-hull simulations are made for estimating nominal hull wake fields by URANS solver. Cavitation simulations are made on the propeller and rudder by DES with a cavitation model and an Eulerian multiphase flow model. Nominal hull wake is numerically modelled in cavitation simulations as a propeller inflow instead of including a hull model. The maximum cavity area on the suction side of the blade is increased by 19 – 32% for beam, stern-quartering and following sea waves compared to calm water mostly due to the stronger axial hull wake. As the sheet cavity is more extended, tip vortex cavitation is intensified especially for stern-quartering and following waves. The maximum cavity area is on a similar level with less than 3% differences for head and bow waves as for calm water. The CFD investigation shows that hull wake differs depending on the wave direction and it can lead to significant changes in cavitation safety.

Keywords: ship propeller; cavitation; CFD; hull wake; wave heading; KCS.

NOMENCLATURE

A_{Cav}	Cavity area over the blade surface [m^2]
A_E	Expanded blade area [m^2]
A_O	Propeller disk area [m^2]
B	Maximum ship breadth of waterline [m]
C	Blade chord length [m]
C_P	Pressure coefficient [-]
D	Propeller diameter [m]
D_{Hub}	Propeller hub diameter [m]

g Gravitational acceleration [m s^{-2}]
$h_{0.7R}$ Blade immersion depth at $0.7 \cdot R$ in the upright position [m]
J Propeller advance ratio [-]
K_T Propeller thrust coefficient [-]
L_{PP} Ship length between perpendicular [m]
N Propeller speed [m s^{-1}]
P_{Atm} Atmospheric pressure [Pa]
P_{Mean} Mean propeller pitch [m]
P_{Ref} Reference pressure [Pa]
P_V Vapour pressure [Pa]
R Propeller radius [m]
T_A Ship draught [m]
T_e Wave encounter period [s]
V_S Ship speed [m s^{-1}]
w Effective wake fraction [-]
w_T Nominal wake fraction [-]

α_V Vapour volume fraction [-]
Δ Ship displacement volume [m^3]
θ_B Blade angular position [°]
θ_w Wave heading [°]
ρ Water density [kg m^{-3}]
σ_N Cavitation number [-]

CFD Computational Fluid Dynamics
DES Detached Eddy Simulation
KCS KRISO Container Ship
LES Large Eddy Simulation
URANS Unsteady Reynolds-Averaged Navier-Stokes

1. INTRODUCTION

Ship propulsion systems are designed mainly for calm water operations because ship performance is verified in sea trials at specified loading conditions ideally with no waves. As ships operates under sea wave conditions most of time, sea margins are added to calm water power for considering sea states and other environmental effects. The sea margin is estimated based on operational profiles and voyage routes in a range of 10 – 30% (MAN 2018).

As the effect of waves is one of the major contributors to the sea margin, there have been increasing research on ship performance in waves. Most studies are focused on added resistance, seakeeping and maneuverability in head sea waves. Extensive experimental studies have been made on three hull types in four model test facilities to investigate added resistance, ship motion and course-keeping ability for different wave lengths and headings (Sprenger *et al.* 2017). The comparison of numerical predictions using potential flow and CFD solvers with experimental results on added resistance and ship motion for KRISO container ship (KCS) has shown a good agreement in added resistance and ship motion for calm water and head sea waves and relatively larger deviations for other wave headings (Sadat-Hosseini *et al.* 2015). The CFD prediction of added resistance and ship motion on KCS has been improved to be within experimental uncertainty for variable wave headings (Mikkelsen *et al.* 2021).

When considering sea waves in the ship propeller design, it is important to take into account not only added resistance but hull wake fields as propeller inflows in predicting propulsive performance and cavitation safety. There is a limited number of studies on propeller performance for different wave headings. Numerical predictions of propeller performance in non-cavitating and cavitating conditions have been made by using a potential flow method coupled with a viscous flow method computation of hull flows in head sea waves (Saettone *et al.* 2020). Nominal hull wake has been computed by bare-hull simulations on KCS for variable wave headings to investigate differences in propeller incidence angle (Mikkelsen *et al.* 2022).

In this work, unsteady cavitation simulations are made on a five-bladed propeller of KCS in calm water and regular waves of five different headings by a DES solver with a multiphase flow model. The nominal hull wake fields from the bare-hull simulations (Mikkelsen *et al.* 2022) are applied to the propeller inflow of the cavitation simulation in an uncoupled way. It is practical in terms of computational effort for resolving unsteady cavitation depending on the blade angular position especially in case of a long wave with a period much longer than that of propeller rotation, but it is disadvantageous in taking into account the interaction of hull wake and upstream propeller perturbation. First, a cavitation simulation is made on the KCS propeller with the hull wake of a dummy hull used in a cavitation tunnel test. The cavitation simulation result is validated against the experimental result. Next, the hull wake field showing the highest wake fraction is taken from the bare-hull simulation for variable wave headings and it is applied to the cavitation simulation. The cavity extent over the blade surface and the sectional pressure distribution are compared between calm water and different wave headings.

2. TEST CASE

The test case is the 5-bladed fixed-pitch KP505 propeller of the 3,600 TEU KCS. It is a well-known benchmark case considered for bare-hull, self-propulsion and maneuvering simulations in CFD and SIMMAN workshops (Hino *et al.* 2020, Simonsen *et al.* 2017). It is often used as a test case of ship performance predictions for variable wave lengths and headings (Sadat-Hosseini *et al.* 2015, Sanada *et al.* 2018).

In Tab. 1, the main particulars of KCS and KP505 are listed. The hull model size in maneuvering and seakeeping basins with a wave generator in different headings is generally smaller than in deep-water basins for resistance and self-propulsion tests and in large-size cavitation tunnels. The bare-hull simulation setup follows the scale ratio of the maneuvering and seakeeping basin and the cavitation simulation adopts the larger model size.

Table 1. Main particulars of KCS and KP505

				Full scale	Model scale	
					Bare-hull	Cavitation
Ship	Length between perpendicular	L_{PP}	[m]	230.0	3.200	7.279
	Maximum breadth of waterline	B	[m]	32.2	0.448	1.019
	Even keel draught	T_A	[m]	10.8	0.150	0.342
	Displacement volume	Δ	[m^3]	52030.0	0.140	1.649
Propeller	Diameter	D	[m]	7.90	0.110	0.250
	Hub diameter	D_{Hub}	[m]	1.42	0.020	0.045
	Mean pitch ratio	P_{Mean}/D	[-]		0.95	
	Expanded area ratio	A_E/A_O	[-]		0.80	

In Tab. 2, the test condition is presented. V_S and N are scaled down by Froude's law in the bare-hull simulations, whereas N is set to 30 rps in cavitation simulations for reaching a higher Reynolds number than in towing tank tests and V_S is adjusted to have the same value of J as in full scale, where $J = V_S \cdot (1 - w)/N$. N, w and K_T are obtained from a self-propulsion model test result (Fujisawa *et al.* 2000), where $K_T = T / (\rho \cdot N^2 \cdot D^4)$. The cavitation number σ_N is defined by $\sigma_N = (P_{Atm} + \rho \cdot g \cdot h_{0.7R} - P_V)/(0.5 \cdot \rho \cdot N^2 \cdot D^2)$ and $h_{0.7R}$ includes the stern wave height. $K_T = 0.170$ and $\sigma_N = 1.609$ are for calm water.

Table 2. Test condition

			Full scale		Model scale			
					Bare-hull		Cavitation	
Ship speed	V_S		24.0	kn	1.457	m/s	6.938	m/s
Propeller speed	N		101.4	rpm	14.3	rps	30.0	rps
Effective wake fraction	w	[-]			0.208			
Thrust coefficient	K_T	[-]			0.170			
Cavitation number	σ_N	[-]			1.609			

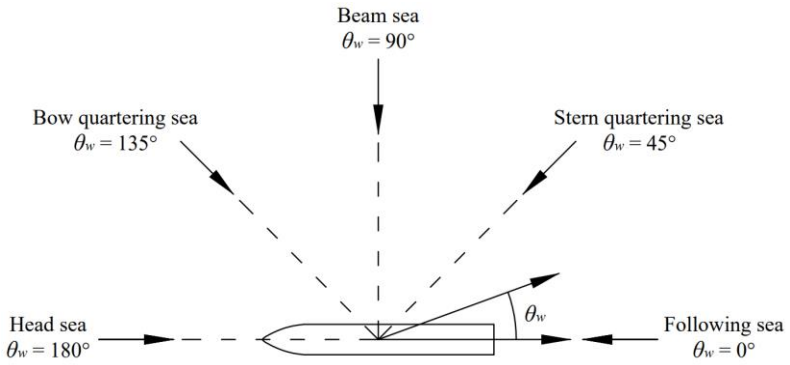

Figure 1. Five wave headings considered in the bare-hull and cavitation simulations

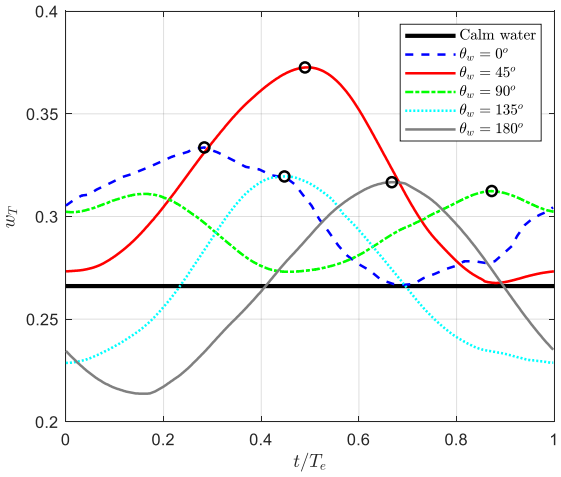

Figure 2. Nominal wake fraction variation over one encounter period T_e for five wave headings in the bare-hull simulations (Mikkelsen *et al.* 2022)

The fifth-order Stokes wave is considered in five headings as shown in Fig. 1. The wave steepness is 1/60 and the wave length is the same as the ship length. In Fig. 2, the variation of nominal wake fraction w_T in the bare-hull simulations of Mikkelsen *et al.* (2022) for calm water and waves of different headings is presented. The variation is over one wave encounter period T_e, which is the same as the incident wave period for beam wave and shorter for head and bow-quartering waves. The wave crest is on the forward perpendicular at $t/T_e = 0$.

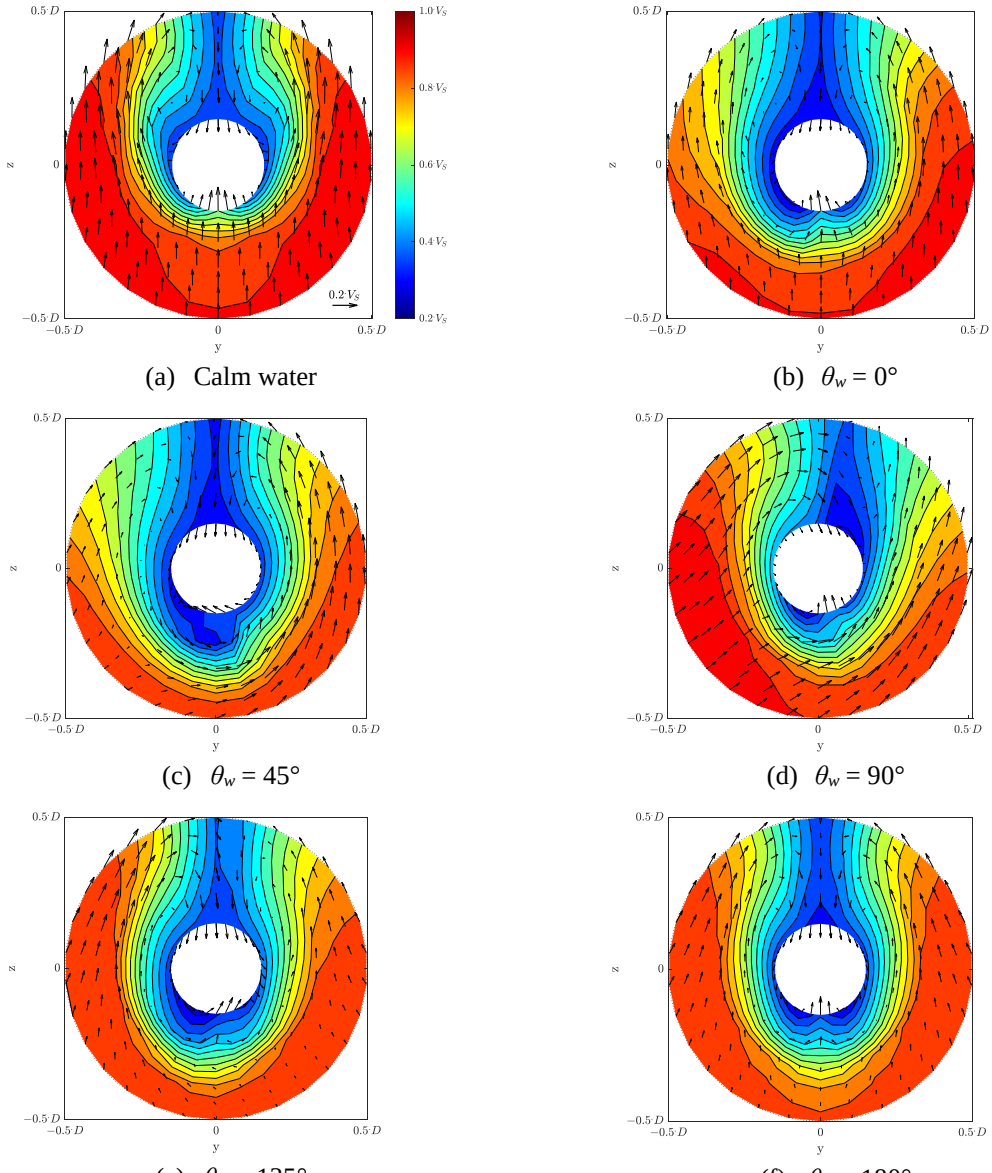

(a) Calm water (b) $\theta_w = 0°$

(c) $\theta_w = 45°$ (d) $\theta_w = 90°$

(e) $\theta_w = 135°$ (f) $\theta_w = 180°$

Figure 3. Hull wake at the highest value of w_T in the bare-hull simulations (Mikkelsen *et al.* 2022)

The overall value of w_T is higher for following, stern-quartering and beam waves. It is the highest for stern-quartering wave. The mean value of w_T for bow-quartering and head waves is close to that for calm water. As the cavity extent is larger for stronger hull wake as a rule, the hull wake field at the

highest value of w_T indicated by circle marks in Fig. 2 is considered in cavitation simulations. As invariable hull wake is applied to cavitation simulations, the dynamic effect of variable hull wake on the propeller flow is not taken into account. Variable hull wake probably has a minor effect especially for stern-quartering and following waves because there are around 40 propeller rotations for one wave encounter period. In Fig. 3, the hull wake at the highest value of w_T is presented. The high wake regions at the 12 o'clock position are widened in waves compared to those in calm water. The axial wake below the hub is stronger in waves for θ_w = 45°, 135°, 180°, as the wave trough is near the stern. While axial and transverse wake is symmetric in calm water and head wave, it is not symmetric for the other wave headings due to oscillating bilge vortex.

3. CFD SETUP

The DES solver of the commercial CFD software StarCCM+ is adopted for unsteady cavitation simulations. In DES, detached flow regions are solved by LES and the rest of flow regions is solved by RANS with the k-ω SST turbulence model. The VOF method is used for modelling multiphase flows. Cavitation is modelled by the interphase mass transfer model of Schnerr and Sauer (2001).

Cavitation simulations are made on propeller and rudder models in a cylindrical fluid domain, as shown in Fig. 4. An inner cylindrical subdomain is defined around the propeller for modelling propeller rotations by the rigid body motion and the sliding grid. The surface grid size is 0.25 – 0.5 mm on the overall propeller surface and it is refined to 0.1 – 0.25 mm along the blade edges. A trimmed hexahedral grid is prepared for the volumetric grid in the fluid domain. The volumetric grid at the outer radius region is refined to have a consistent grid size around 0.2 mm. Wall boundary regions are resolved by the prism-layer grid resulting in non-dimensional wall distances mostly below 2.

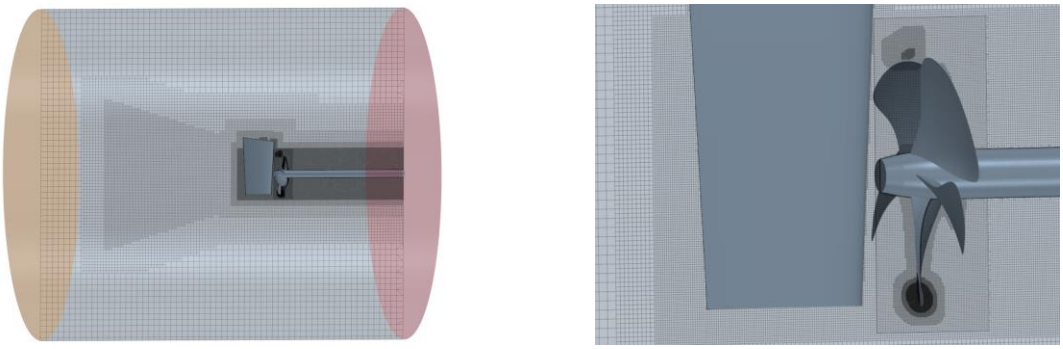

(a) (b)

Figure 4. (a) Computational domain, (b) Propeller and rudder models with volumetric grid on a vertical section in cavitation simulations

The nominal hull wake obtained from the bare-hull simulations in Fig. 3 is applied to the cavitation simulation as a propeller inflow instead of including a hull model (Shin *et al.* 2015). The axial wake is scaled down by the ratio of w/w_T and is applied to the inlet boundary condition. The transverse wake consisting of radial and tangential wake components is modelled by momentum sources applied about $0.4 \cdot D$ upstream from the propeller plane. Momentum source strengths are iteratively adjusted by numerical tests in the same computational domain as used in the cavitation simulation performed without including the propeller model.

The reference pressure P_{Ref} obtained from $P_{Ref} = 0.5 \cdot \rho \cdot N^2 \cdot D^2 \cdot \sigma_N + P_V$ for the model-scale values of N and D is applied to the cavitation simulation. Unsteady simulations are made with a 2nd-order implicit time-stepping scheme and a time step corresponding to 0.5° propeller rotation per time step. The same values of N and V_S are applied to the cavitation simulations in calm water and waves.

The CFD method adopted in this study for simulating ship propeller cavitation in the behind-hull condition has been validated against experimental results of large-size cavitation tunnel tests including a hull model for different cavitation types and cavitation-related issues (Shin and Andersen 2018, 2019, 2020).

4. VALIDATION OF CAVITATION SIMULATION

A cavitation simulation is made on the KP505 propeller with hull wake used in the cavitation tunnel test and it is validated against the experimental result (Heinke and Jaksic 2003). The axial hull wake shown in Fig. 5 is generated by a dummy hull and screens. Since transverse wake is not included in the simulated hull wake, momentum sources are not applied to the cavitation simulation. The condition of $J = 0.716$ and $\sigma_N = 1.536$ is considered, and the propeller loading and cavitation susceptibility are slightly higher than the test condition in Tab. 2.

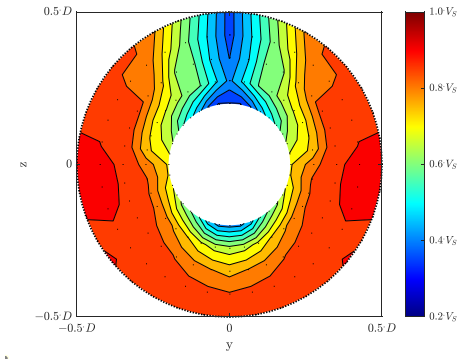

Figure 5. Hull wake simulated in the cavitation tunnel test

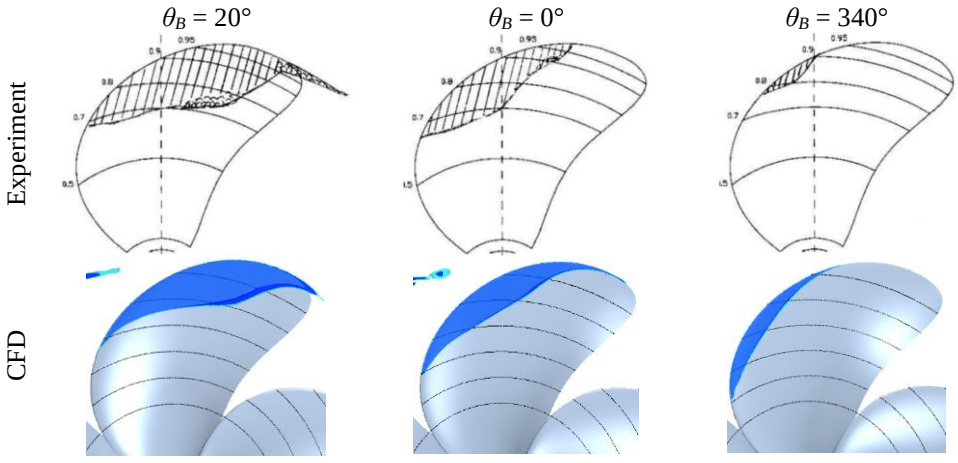

Figure 6. Cavitation on the suction side of the blade in the experiment (Heinke and Jaksic 2003) and CFD

In Fig. 6, the cavitation simulation is compared with the experimental result. In CFD, the cavity interfaces indicated by light and dark blue contours are defined by the iso-surfaces of α_V = 10% and 50%, respectively. CFD shows reasonable agreement in the overall extent of sheet and tip vortex cavitation. The radial extent of the leading-edge sheet cavitation is overpredicted at θ_B = 340° and the chordwise extent of the sheet cavitation is underpredicted at θ_B = 0° and 20°, where θ_B = 0° is the 12 o'clock position.

5. CAVITATION SIMULATIONS IN WAVES

Cavitation simulations are made with the hull wake fields in calm water and waves of different headings. Unsteady simulations are run until the propeller thrust and torque are periodically converged. In Fig. 7, the one-blade thrust variation is presented with respect to the blade position. The maximum value of $K_{T,1B}$ is shown near θ_B = 0°, where the axial wake peak is. The mean value of K_T for calm water is close to K_T = 0.170 in the test condition with a deviation less than 1%. The mean $K_{T,1B}$ is 10 – 24% higher for waves than for calm water due to the increased inner-radius wake, whereas the maximum $K_{T,1B}$ is 5 – 7% higher for θ_w = 0° & 45° and 4% lower for θ_w = 135° and on a similar level for θ_w = 90° & 180°. There is no indication of thrust breakdown for waves.

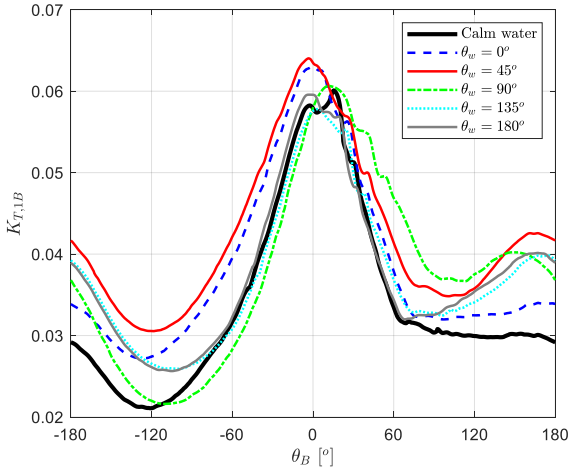

Figure 7. One-blade thrust coefficient with respect to the blade position for calm water and waves

In Fig. 8 & 9, the comparison of the cavity distribution is presented for calm water and waves of different headings. Leading-edge sheet cavitation starts at $\theta_B \approx$ -40° in calm water and earlier at $\theta_B \approx$ -60° – -50° in following and stern-quartering waves. Sheet cavitation is extended radially towards the inner radius and along the chord until $\theta_B \approx$ 20° and it has further chordwise extension in the outer radius at $\theta_B \approx$ 20° – 40°. Sheet cavitation is gradually converted to tip vortex cavitation. For following and stern quartering waves, sheet cavitation is more extended along the radial and chordwise directions and tip vortex cavitation is stronger than for calm water. Sheet cavitation detachment is so intense that a double vortex structure is formed in tip vortex cavitation at $\theta_B \approx$ 60°. For beam wave, leading-edge sheet cavitation starts later and sheet cavitation is more extended along the radial direction at the later blade positions due to the stronger hull wake on the starboard side. For head and bow quartering waves, sheet cavitation have a similar extent as for calm water and tip vortex cavitation looks a bit more intensified at $\theta_B \approx$ 80°.

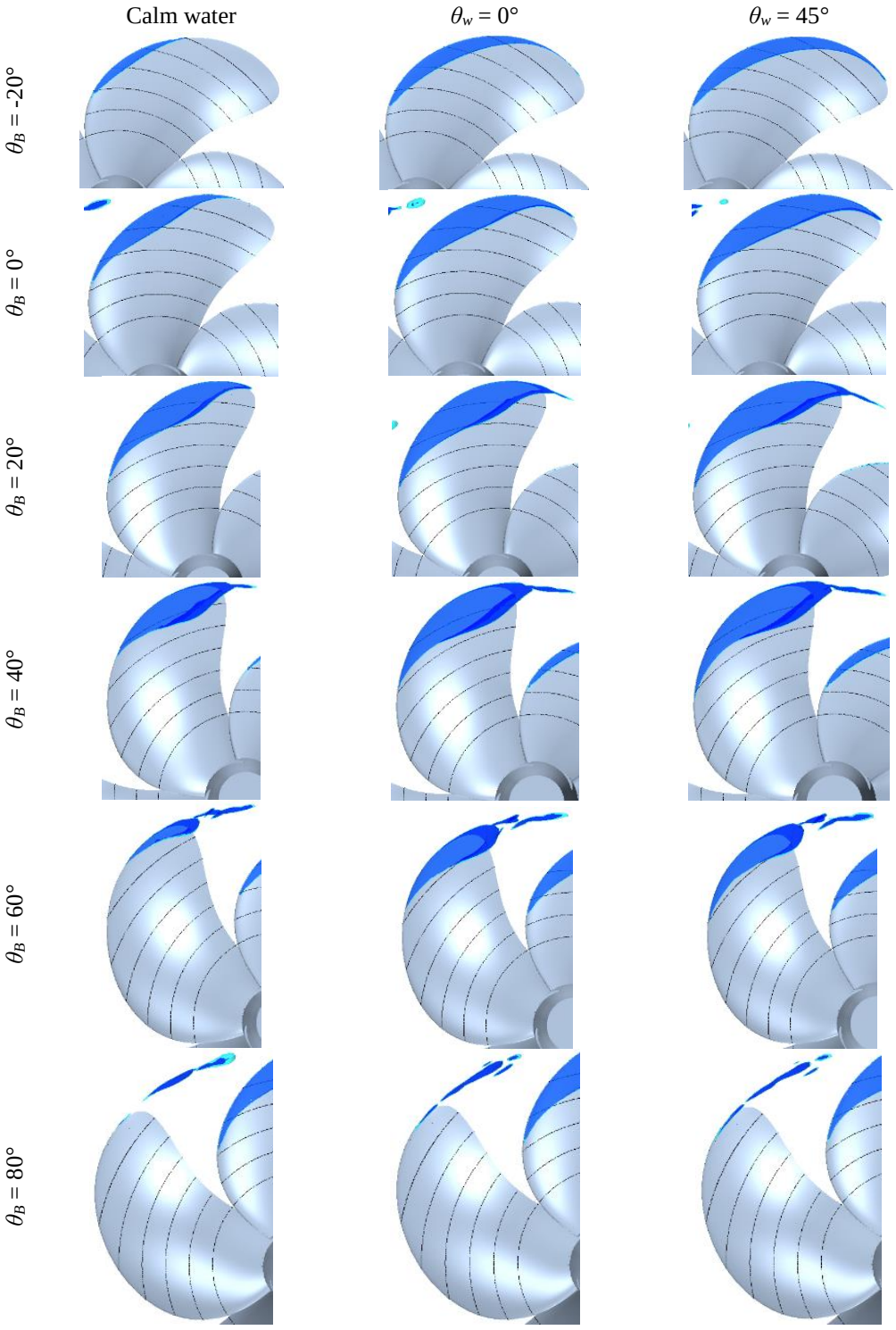

Figure 8. Cavitation on the suction side of the blade for calm water, following and stern-quartering sea waves

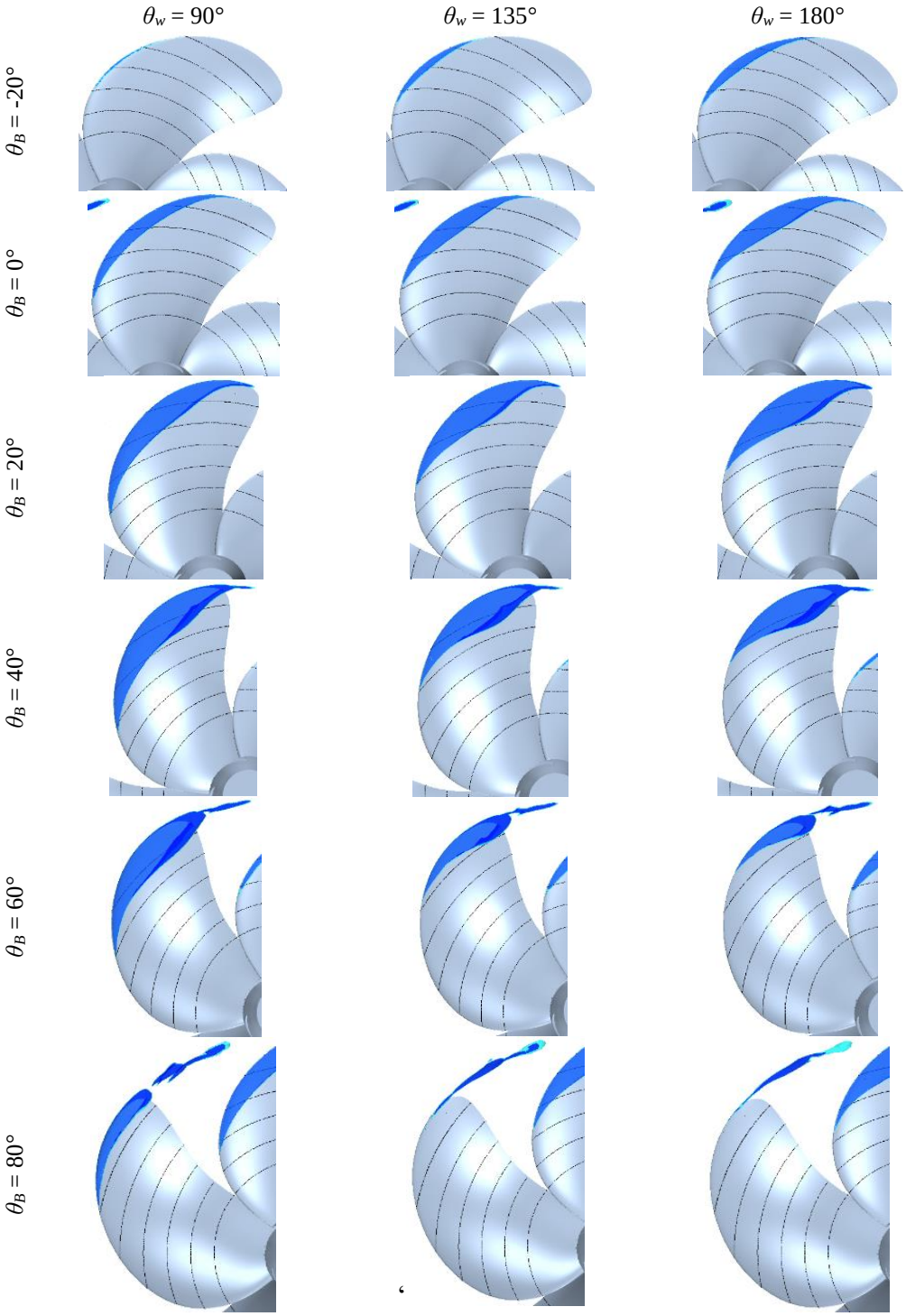

Figure 9. Cavitation on the suction side of the blade for beam, bow-quartering and head sea waves

In Fig. 10, the variation of the cavity area over the suction-side blade surface is presented with respect to the blade position. The maximum cavity area is increased by 27 – 32% for following and stern-quartering waves compared to calm water. The maximum cavity area is shown at $\theta_B \approx 20°$ later than θ_B

≈ 0° showing the maximum one-blade thrust because it takes a time to build up a cavity after passing the wake peak. For beam wave, the cavity area curve is shifted by about 20° compared to calm water and other wave headings due to the stronger wake on the starboard side and the maximum cavity area is 19% larger than for calm water. For head and bow quartering waves, the maximum cavity area is on a similar level within 4% differences as for calm water.

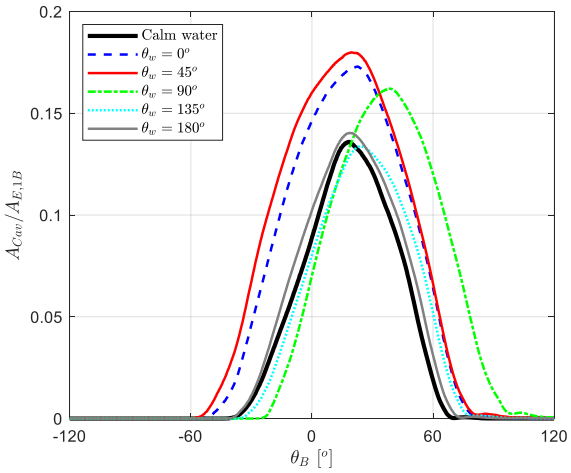

Figure 10. Cavity area over the blade surface in calm water and waves

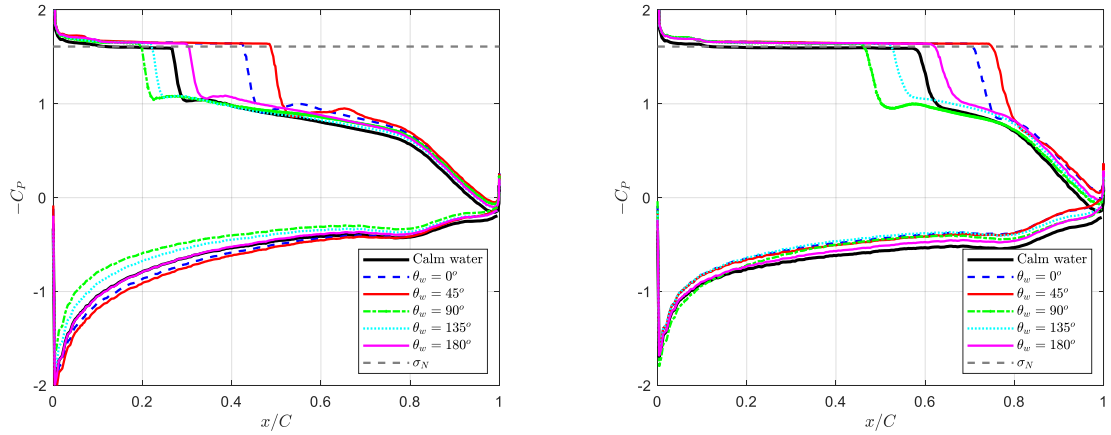

(a) (b)

Figure 11. Sectional pressure distribution on 0.9·R along the chord: (a) θ_B = 0°, (b) θ_B = 20°

In Fig. 11, the pressure coefficient C_P on the section of 0.9·R is presented, where C_P = (P – P_{Ref})/(0.5·ρ·N^2·D^2). As the vertical axis is for -C_P, the upper curve corresponds to the pressure distribution on the suction side. The constant pressure region near σ_N on the suction side is under the sheet cavity. The constant pressure is slightly above σ_N for waves because the stern wave height is larger than for calm water. The region under the sheet cavity is longer for following and stern-quartering waves and shorter for bow-quartering and beam waves than for calm water. C_P on the pressure side is lower for bow-quartering and beam waves at θ_B = 0°, which indicates that the angle of attack is lower than for calm water and other wave headings.

6. CONCLUSIONS

Cavitation simulations are made on the propeller and rudder models with the hull wake taken from the bare-hull simulations for calm water and waves of five different headings.

- The uncoupled approach for simulating hull and propeller flows separately is a practical way in terms of computational effort for estimating cavitation safety in case of long-period waves.

- For following and stern-quartering waves, the maximum area under sheet cavitation is about 30% larger than for calm water, but the maximum one-blade thrust is increased only by about 5%. As sheet cavitation is more extended, tip vortex cavitation is also intensified.

- For beam wave, the maximum cavity area is increased by about 20% because of the stronger hull wake on the starboard side, even though the maximum one-blade thrust is on a similar level as for calm water. The cavitation growth has about 20° delay compared to calm water and other wave headings due to the asymmetric hull wake.

- For head and bow-quartering waves, the maximum cavity area and the one-blade thrust are on similar levels as for calm water.

- There is a significant change of cavitation safety depending on the wave direction. It is necessary to take into account the wave effect on cavitation safety in designing ship propellers exposed to severe wave conditions.

REFERENCES

Fujisawa, J., Ukon, Y., Kume, K. and Takeshi, H. (2000). *Local Velocity Field Measurements around the KCS Model*. SRI M.S. No. 631

Heinke, H.J. and Jaksic, D. (2004). Kavitationsuntersuchungen und Druckschwankungsmessungen mit fünf Propellern am Dummymodell des KRISO Containerschiffs KS 621. Technical Report 3036, SVA, Potsdam, Germany.

Hino, T., Stern, F., Larsson, L., Visonneau, M., Hirakata, N. and Kim, J. (2020). *Numerical Ship Hydrodynamics: An Assessment of the Tokyo 2015 Workshop*. Springer-Verlag.

MAN Energy Solutions (2018). *Basic Principles of Ship Propulsion*. Copenhagen, Denmark.

Mikkelsen, H., Shao, Y. and Walther, J. H. (2021). CFD verification and validation of added resistance and seakeeping response in regular oblique waves with varying wave length. Proc. of MARINE 2021.

Mikkelsen, H., Shao, Y. and Walther, J. H. (2022). Numerical Study of Nominal Wake Fields of a Container Ship in Oblique Regular Waves. Applied Ocean Research, 119.

Saettone, S., Taskar, B., Regener, P. B., Steen, S., and Andersen, P. (2020). A Comparison between Fully-unsteady and Quasi-steady Approach for the Prediction of the Propeller Performance in Waves. Applied Ocean Research, 99, 1–16.

Sanada, Y., Kim, D. H., Sadat-Hosseini, H., Toda, Y., Simonsen, C. and Stern, F. (2018). Experiment and Numerical Simulation for KCS Added Powering in Regular Head/Oblique Waves. Proc. of 32nd Symposium on Naval Hydrodynamics, Hamburg, Germany.

Schnerr, G.H. and Sauer, J. (2001) Physical and numerical modeling of unsteady cavitation dynamics. Proc. of 4th Int. Conf. on Multiphase Flow (ICMF2001), New Orleans, LA, USA.

Simonsen, C., Otzen, J., Quadvlieg, F. and Stern, F. (2017). *Proceedings SIMMAN 2014 Workshop*. Copenhagen, Denmark.

Shin, K.W., Regener, P.B. and Andersen, P. (2015). Methods for cavitation prediction on tip-modified propellers in ship wake fields. Proc. of smp'15, Austin, Texas, USA.

Shin, K.W. and Andersen, P. (2018). CFD analysis of propeller tip vortex cavitation in ship wake fields. Proc. of CAV2018, Baltimore, MD, USA.

Shin, K.W. and Andersen, P. (2019). CFD analysis of ship propeller thrust breakdown. Proc. of smp'19, Rome, Italy.

Shin, K.W. and Andersen, P. (2020). Practical Numerical Method for Erosion Risk Prediction on Ship Propellers. Int. Shipbuilding Progress, 67:199-220.

Sprenger, F., Maron, A., Delefortrie, G, Zwijnsvoorde, T.V., Cura-Hochbaum, A., Lengwinat, A. and Papanikolaou, A. (2017). Experimental Studies on Seakeeping and Maneuverability of Ships in Adverse Weather Conditions. J. Ship. Res. 61 (3), 131–152.